ACS Catalysis

Research Article

Cite This: ACS Catal. 2019, 9, 11386−11397

pubs.acs.org/acscatalysis

Di-Palladium Complexes are Active Catalysts for Mono-N-Protected Amino Acid-Accelerated Enantioselective C−H Functionalization

Joseph J. Gair,[‡] Brandon E. Haines,[∥] Alexander S. Filatov,[‡] Djamaladdin G. Musaev,*[,§] and Jared C. Lewis*[,†]

[†]Department of Chemistry, Indiana University, Bloomington, Indiana 47405, United States

[‡]Department of Chemistry, University of Chicago, Chicago, Illinois 60637, United States

[§]Cherry L. Emerson Center for Scientific Computation, Emory University, Atlanta, Georgia 30322, United States

[∥]Department of Chemistry, Westmont College, Santa Barbara, California 93108, United States

Supporting Information

ABSTRACT: The role of mono-protected amino acid (MPAA) ligands in accelerating enantioselective cyclopalladation and palladium-catalyzed C−H functionalization was investigated using kinetic, spectroscopic, and computational methods. The catalytic relevance of characterized di-palladium species was evaluated by kinetic analysis. The kinetic method of continuous variation (MCV) demonstrated that a complex containing a single MPAA-bridged di-palladium core ($Pd_2(MPAA)_1$) is an active catalyst for the reactions studied. The experimental findings are consistent with density functional theory calculations that indicate that enantioinduction can be achieved by a single MPAA ligand bridging a di-palladium catalyst through secondary sphere hydrogen-bonding interactions that lower the barrier to C−H activation of the major enantiomer.

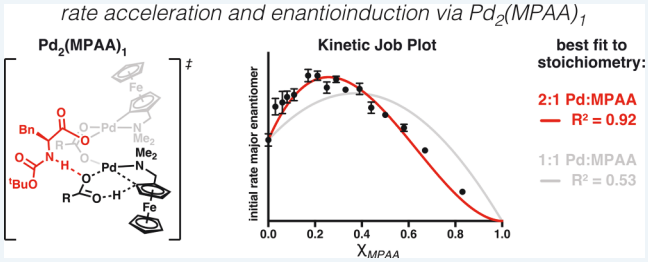

KEYWORDS: *MPAA, bimetallic, ligand-accelerated, asymmetric catalysis, MCV*

INTRODUCTION

Understanding how attractive interactions accelerate specific chemical reactions and thus enable selective catalysis is a central goal of catalysis science.[1−4] Achieving this goal requires insight into the structure of the active catalyst(s) for a reaction, but obtaining this information is often complicated by the formation of dynamic ensembles of catalysts in low concentrations within complex reaction mixtures. Reaction kinetics and density functional theory (DFT) calculations, when informed by accurate information regarding precatalyst structure and speciation, provide a means to evaluate the feasibility of different catalyst architectures. In this work, we leverage these tools to elucidate the di-palladium structure of a catalyst for enantioselective C−H functionalization. These structural insights provide the framework for a revised model of stereoinduction via stabilizing hydrogen-bonding interactions in the secondary coordination sphere that accelerate enantioselective C−H activation.

Mono-protected amino acid (MPAA) ligands have led to significant advances in palladium-catalyzed C−H functionalization as a result of their ability to enhance reaction rates and to impart enantioselectivity to a range of transformations.[5−15] Early studies by Reutov established that MPAA ligands enable enantioselective cyclopalladation of *N*,*N*-dimethylaminomethylferrocene (**1**, dmaf) (Figure 1A).[16] Since this discovery, dmaf (**1**) has served as a representative substrate in stoichiometric,[17−21] computational,[22] and catalytic[23−29] studies of MPAA ligands in enantioselective cyclopalladation.[30−33] Yu reported the first instance in which MPAA ligands were used [in conjunction with Pd(II)] for catalytic enantioselective C−H functionalization in the desymmetrization of benzhydryl pyridines (bhp) (Figure 1B).[34] This study also provided a model for stereoinduction via bidentate MPAA coordination on the basis of a reported[35] bidentate MPAA palladacycle (Figure 1C).

The bidentate model was supported by the observation that *N*-methyl ligands afforded minimal enantioinduction.[34] The hypothesis that bidentate MPAA coordination could enable rate acceleration and stereoinduction was subsequently corroborated by DFT calculations,[37−40] observation of Pd−MPAA ions via high-resolution mass spectrometry,[41−45] first-order dependence on total palladium in steady-state kinetics,[46,47] and a lack of nonlinear effects (NLE) in asymmetric reactions.[48,49] As indicated by its frequent reproduction in review literature,[5,14,23,50−60] the bidentate model has been widely adopted as a general mechanism to rationalize rate acceleration and stereocontrol in Pd−MPAA catalysis.

Received: September 10, 2019
Revised: October 29, 2019
Published: October 31, 2019

DOI: 10.1021/acscatal.9b03887
ACS Catal. 2019, 9, 11386−11397

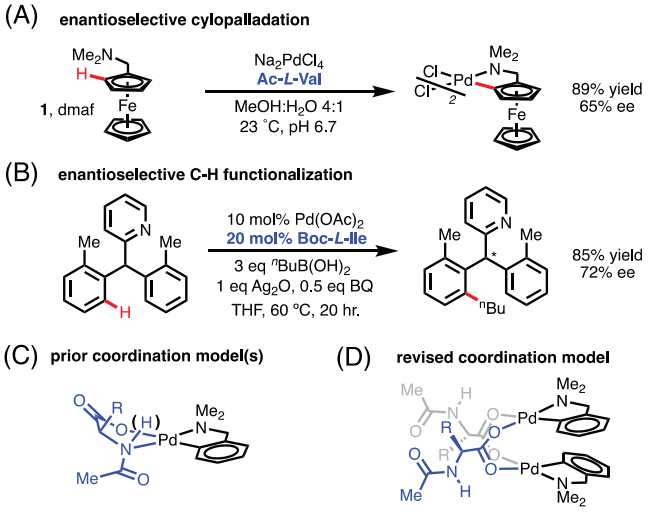

Figure 1. Seminal reports of MPAA ligands in (A) enantioselective cyclopalladation[16] and (B) palladium-catalyzed asymmetric C−H functionalization.[34] (C) Previously reported model for bidentate MPAA coordination.[35] (D) Revised model of MPAA coordination.[36]

Given the prevalence of the bidentate model in the literature, we were surprised when our attempts to prepare the complex on which it was originally based[35] afforded an MPAA-bridged dimer (Figure 1D).[36] A wide range of carboxylate-bridged complexes have been structurally characterized,[61−67] and carboxylate-bridged di-palladium complexes have been proposed as key intermediates in catalytic reactions,[68,69] but our report was the first to show that the MPAA carboxylate moiety also adopts this coordination mode.[36] Indeed, our study revealed that MPAA-bridged di-palladium complexes are the only species observable in solution for palladacycles of *N*,*N*-dimethylbenzylamine (dmba), but exchange experiments indicated that high-energy mono-palladium complexes were likely also present in the solution. Given that mono- and di-palladium complexes (Figure 1C,D) possess distinct structures with their own unique potential for interacting with substrates, we wished to establish whether di-palladium complexes[61,63,68−72] are active catalysts for enantioselective C−H activation/functionalization of prototypical substrates [e.g. *N*,*N*-dimethylaminoferrocene (**1**) and bhp].

RESULTS AND DISCUSSION

Di-Palladium Complexes and dmaf Olefination. Asymmetric olefination of dmaf (**1**) with *N*,*N*-dimethylacrylamide (**2**) was selected as a model reaction for kinetic studies because data acquisition was expedited by the operational simplicity of conducting reactions open to air (O_2 terminal oxidant, Figure 2A).[28,73] The reaction was optimized for mechanistic analysis by omitting bromide additives, which were not required for high levels of enantioinduction. The absolute chirality of the major product enantiomer from this reaction (*S*) was determined by SXRD (**3**, Figure 3B), and major enantiomer formation was quantified using chiral stationary phase supercritical fluid chromatography (SFC). The structure and speciation of dmaf palladacycles in solution were also established and found to be consistent with the di-palladium complexes observed in our previous work (Figures S5−S23).[36] Of particular importance is the observation that acetate-bridged palladacycle **4** undergoes rapid, sequential

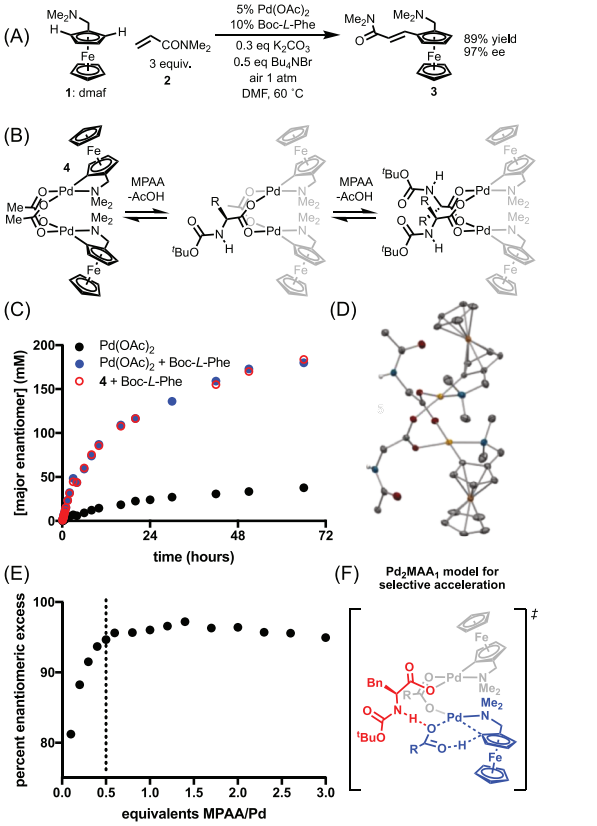

Figure 2. (A) Model reaction for kinetic analysis. (B) Observation of sequential MPAA ligand substitution upon titration of palladacycle **4**. (C) Mixtures of palladacycle **4** + MPAA form catalysts that are kinetically competent for acceleration of the major enantiomer relative to palladium(II) acetate alone. (D) ORTEP of palladacycle **5** with 40% thermal ellipsoids. (E) Maximal rate acceleration is achieved with only 0.5 equiv of MPAA per palladium. (F) Proposed model for Pd_2MPAA_1 catalysis.

ligand substitution upon titration with MPAA (Figures 2B and S17−S21). In the presence of excess MPAA, the ligand exchange equilibrium can be driven to favor di-MPAA complexes (e.g. palladacycle **5**, Figure 2D). The observed ligand exchange is suitable for generating kinetically competent catalysts that provide marked rate acceleration relative to $Pd(OAc)_2$ from the acetate-bridged palladacycle **4** (Figures 2C and S4). Given that palladacycle **4** is a suitable precatalyst for enantioselective C−H functionalization, we next endeavored to identify the active catalyst in dehydrogenative olefination of dmaf.

Preliminary experiments revealed that only 0.5 equiv of MPAA per Pd are required to achieve maximal enantiomeric excess (ee) for dmaf olefination (Figure 2E). This observation led us to hypothesize that rate acceleration and stereocontrol in dmaf olefination may be achieved by a di-palladium catalyst wherein only one MPAA ligand [i.e., $Pd_2(MPAA)_1$, Figure 2F] is required to achieve accelerated C−H functionalization of the major enantiomer. Although additional MPAA ligands may be coordinated to the active catalyst(s), these might exhibit only minimal kinetic contributions. Hydrogen bonding in the crystal lattice of **5** and intramolecular hydrogen bonding in computational studies of cyclopalladation[36] led us to hypothesize that secondary sphere hydrogen bonding could stabilize the transition state for enantioselective C−H activation (red ligand in Figure 2F).

DOI: 10.1021/acscatal.9b03887
ACS Catal. 2019, 9, 11386−11397

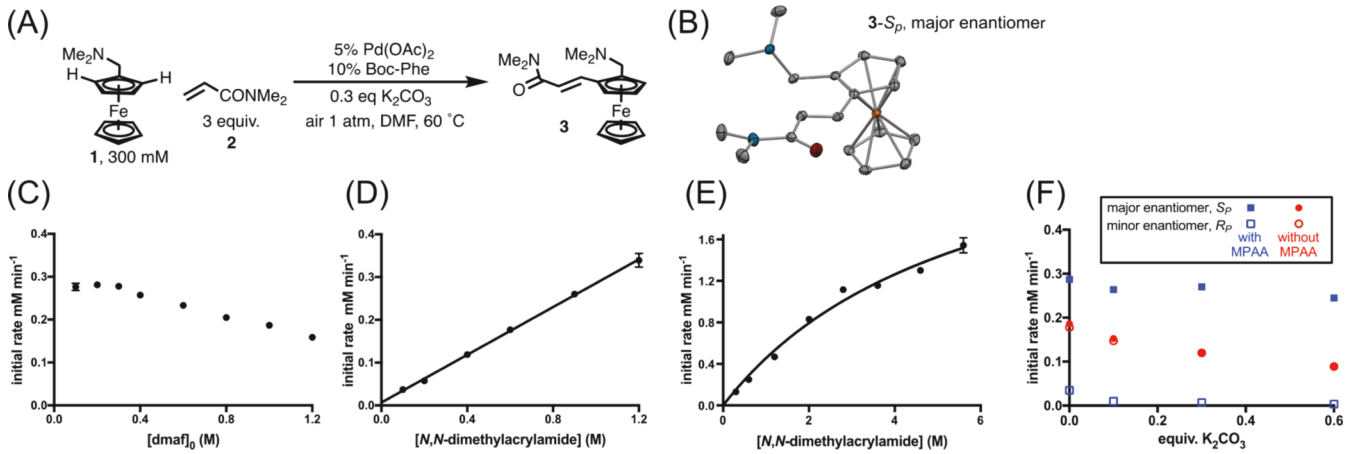

Figure 3. (A) Standard reaction conditions for kinetic studies; (B) absolute chirality of the major enantiomer (S_p) as determined by SXRD: ORTEP with 40% thermal ellipsoids; (C) order in dmaf ≤0; (D) first order in *N,N*-dimethylacrylamide (0.1−1.2 M), fit to $y = mx + b$; (E) saturation behavior in *N,N*-dimethylacrylamide at high concentrations, fit to Michaelis−Menten equation $y = mx/(x + b)$; (F) negative order in K_2CO_3 with modest selectivity for suppression of the racemic background reaction.

Steady-State Kinetics of dmaf Olefination. The first step toward testing the hypotheses outlined above was to examine the effect of reactant concentrations on the rate of dmaf olefination (Figure 3A). Initial rate data were used because catalyst degradation observed during reaction progress kinetic analysis[74] complicated the interpretation of full reaction profiles (Figure S31).[49] The reaction is zero order in dmaf (**1**) under the standard reaction conditions (0.1−0.3 M), but a negative concentration dependence becomes apparent at higher dmaf loading (0.4−1.2 M, Figure 3C). Zero order in dmaf indicates that dmaf association does not contribute to turnover limitation of the Pd−MPAA catalyst, whereas a negative order indicates that an additional dmaf-dependent process inhibits turnover. Negative order in dmaf can be rationalized by our finding that dmaf coordinates **4** to generate an off-cycle complex consistent with bridge-splitting equilibria observed with isolated dimers[75,76] and in systems with bimetallic[77,78] active catalysts (Figures S10−S13). The reaction is first order in *N,N*-dimethyl-acrylamide (**2**) from 0.1−1.2 M, indicating that olefin insertion contributes to limiting the rate of Pd−MPAA turnover (Figure 3D).[79] At higher olefin concentrations, the reaction displays saturation kinetics, consistent with reversible olefin binding prior to insertion (Figure 3E).[80]

In the presence of MPAA, K_2CO_3 has little effect on the rate of Pd−MPAA turnover (Figure 3E, blue squares). If the role of K_2CO_3 is to deprotonate the MPAA N−H to generate di-anionic MPAA chelates (Figure 1C), then K_2CO_3 should be necessary for MPAA-induced rate acceleration and should have little effect on the background reaction. On the contrary, major enantiomer formation is accelerated by MPAA [relative to Pd(II) acetate alone] without K_2CO_3 and at all K_2CO_3 loadings investigated (Figure 3E, blue filled squares > red filled circles). The fact that added base provides no selective acceleration of the MPAA promoted reaction suggests that the role of K_2CO_3 in these reactions is not to generate the active catalyst (via MPAA N−H deprotonation). Instead, increasing K_2CO_3 loading appears to suppress the racemic reaction (Figure 3E, red circles). This K_2CO_3-dependent suppression practically eliminates minor enantiomer formation in the MPAA-catalyzed reaction (Figure 3E, blue empty squares), thereby improving enantioselectivity.

Kinetic Isotope Effects in dmaf Olefination. To gain insight into whether C−H activation contributes to the rate of Pd−MPAA turnover, we next turned to a study of deuterium kinetic isotope effect (KIE) experiments.[81−83] In the absence of the MPAA ligand, dmaf olefination afforded a primary KIE (k_H/k_D = 3.91 ± 0.40, Figure 4A). In the presence of the

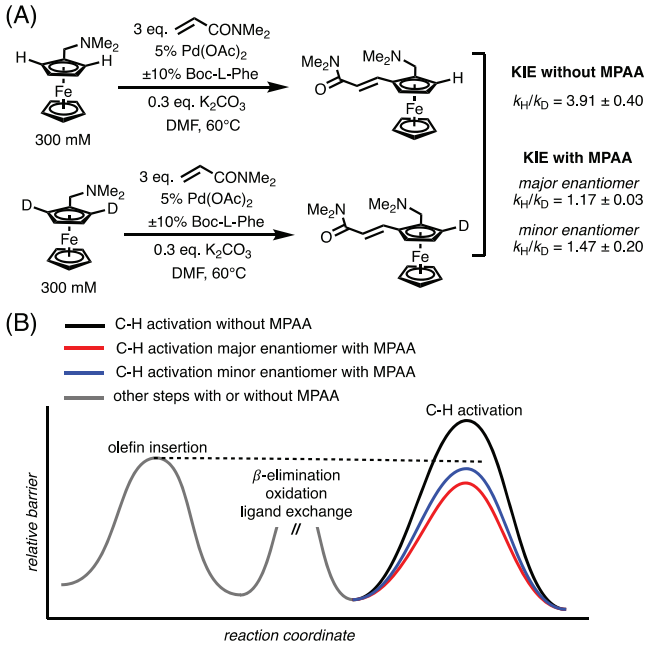

Figure 4. (A) Absolute KIEs with and without the MPAA ligand; (B) qualitative free energy profile summarizing how MPAA ligands change the rate-limiting step in dmaf olefination.

MPAA ligand, on the other hand, a small KIE was observed in the rates of formation of both major and minor enantiomers (k_H/k_D = 1.17 ± 0.03 and 1.47 ± 0.20, respectively). Prior competitive KIE experiments have demonstrated that MPAA ligands lower the barrier to C−H activation.[84] The KIEs, measured by absolute rates in separate experiments,[81] herein are consistent with preliminary studies in a prior report[85] and show that MPAA ligands change the turnover limiting step in palladium-catalyzed C−H olefination of dmaf.

DOI: 10.1021/acscatal.9b03887
ACS Catal. 2019, 9, 11386−11397

The qualitative free energy profile in Figure 4B illustrates a scenario consistent with the observed rates and KIEs. The primary KIE observed without MPAA shows that C−H cleavage is turnover-limiting in the background reaction (Figure 4B, black curve). The fact that MPAA significantly decreases the KIE for both major and minor enantiomers suggests that MPAA lowers the barrier of both product-forming pathways such that they are no longer turnover-limiting (Figure 4B, red and blue curves). Olefin insertion is depicted as turnover-limiting for the Pd−MPAA pathways because of the observed rate dependence on olefin concentration (Figure 3D); however, our experiments do not preclude the possibility of additional slow steps in the catalytic cycle (e.g., β-elimination or O_2 redox chemistry). The small KIE observed in the presence of MPAA could be the result of equilibrium isotope effects, product formation via the background reaction, a different step on the catalytic cycle with a barrier similar to that of C−H cleavage, or a combination of these factors.

Catalyst Stoichiometry during dmaf Olefination. The KIE experiments presented above demonstrate that MPAA ligands change the turnover-limiting step of catalytic dmaf olefination by lowering the barrier to C−H activation. We next sought to identify the species responsible for MPAA-accelerated C−H activation. A plot of ee versus MPAA loading revealed that ee is maximized around a 2:1 Pd:MPAA ratio, consistent with an active catalyst composed of two Pd centers bridged by a single MPAA ligand ($Pd_2(MPAA)_1$) with the second bridging ligand (OAc or MPAA) exerting minimal influence (Figure 2E,F). This abbreviated formula ($Pd_2(MPAA)_1$), used throughout, does not signify that precisely one MPAA ligand is coordinated to the active catalyst but that only one MPAA ligand participates in acceleration of the major enantiomer pathway regardless of the identity of additional coordinated carboxylates.

An NLE experiment was conducted to assess the presence of species containing more than one chiral ligand.[86,87] A small, systematic, positive deviation from linearity was observed in a plot of ee_{MPAA} versus $ee_{product}$, consistent with slightly lower reactivity of $Pd_2(MPAA\text{-}L)_1(MPAA\text{-}D)_1$ relative to $Pd_2(MPAA\text{-}L)_2$ (Figure S55). Notably, the slower rate of the mixed D/L complex is much more apparent in plots of ee_{MPAA} versus rate (Figure S56). Whereas large NLEs result from inequivalent reactivity or stability between diastereomeric catalysts bearing more than one chiral ligand, the small magnitude of the NLE in this work is consistent with the hypothesis that a second bridging ligand (X) in $Pd_2(MPAA)_1(X)_1$ plays only a minor role in determining the rate and selectivity of Pd−MPAA catalysts (the two ligands are stereochemically independent).[88]

To test our hypothesis that MPAA-accelerated C−H activation can be achieved via a $Pd_2(MPAA)_1$ species, we sought to determine the kinetic order in the MPAA ligand. Reactions conducted with 0−1.5 equiv of MPAA ligand per palladium displayed increasing rates of major enantiomer formation and rate acceleration approaching saturation with much less than one MPAA ligand per palladium (Figure 5A). The trend in major enantiomer acceleration is mirrored by concurrent inhibition of minor enantiomer formation. Rate saturation at low MPAA loading qualitatively supports the $Pd_2(MPAA)_1$ hypothesis; however, plotting initial rates versus MPAA loading does not provide a simple kinetic order in MPAA because it reflects competing contributions from two mechanisms (Figure 5B, eqs 1 and 2). On the other hand, our

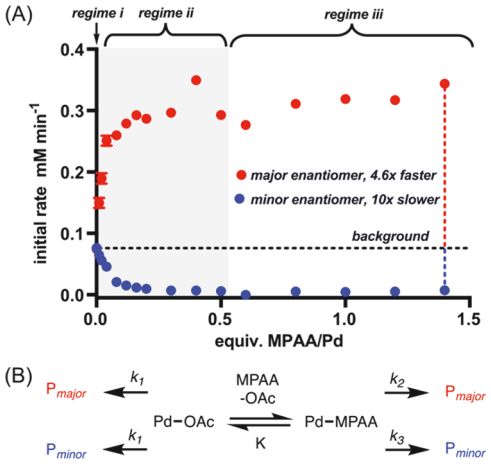

Figure 5. (A) plot of initial rate of major and minor enantiomer formation versus MPAA loading; (B) simplified, minimal model of product-forming pathways.

qualitative observations point to a hypothesis that is testable without complete characterization of the ensemble of resting states; namely, that a species with a relative stoichiometry ($Pd_2(MPAA)_1$) can achieve MPAA-accelerated C−H activation. Toward this end, the kinetic method of continuous variation (MCV) provides a straightforward probe of relative transition state stoichiometry in ligand-accelerated catalysis.

$$\text{Initial rate major enantiomer} = k_1[\text{Pd-OAc}] + k_2[\text{Pd-MPAA}] \quad (1)$$

$$\text{Initial rate minor enantiomer} = k_1[\text{Pd-OAc}] + k_3[\text{Pd-MPAA}] \quad (2)$$

Kinetic MCV Indicates That a $Pd_2(MPAA)_1$ Complex is Responsible for Rate Acceleration in dmaf Olefination. The MCV is well suited for determining the relative stoichiometry of molecular association.[89] Whereas MCV is most frequently used to assess binding equilibria (and thus reactant/product stoichiometry, see Figures S9 and S13) with spectroscopic observables, it can be applied to any molecular association with an experimental observable that is linearly dependent on the concentration of the associated species. In the case of ligand-accelerated, steady-state catalysis, the relevant response is rate (thus probing transition-state stoichiometry).[89] Relevant applications of kinetic MCV to probe transition-state stoichiometry can be found in mechanistic studies of organometallic catalysis,[90−93] enzymology,[94] olefin polymerization,[95] and, most frequently, synthetic models[89,96−102] of metalloenzymes.

The stoichiometry of the MPAA-accelerated transition state was therefore probed using kinetic MCV by plotting the initial rate of major enantiomer formation versus mole fraction MPAA ($\chi_{MPAA} = [MPAA]_0/([MPAA]_0+[Pd(OAc)_2]_0)$) and fitting those data to eq 3, which accounts for the two reactions that contribute to major product formation (for derivation see the Supporting Information eq 34). The relative stoichiometry of palladium with respect to MPAA is represented in eq 3 by the variable a. To reduce the number of adjustable parameters, b was determined independently (b = 1.5, Figure S64).[90,91] Nonlinear least squares curve fitting of the data in Figure 6 to eq 3 gives a best fit $a = 2.03 \pm 0.13$ (constrained to b = 1.5).

DOI: 10.1021/acscatal.9b03887
ACS Catal. 2019, 9, 11386−11397

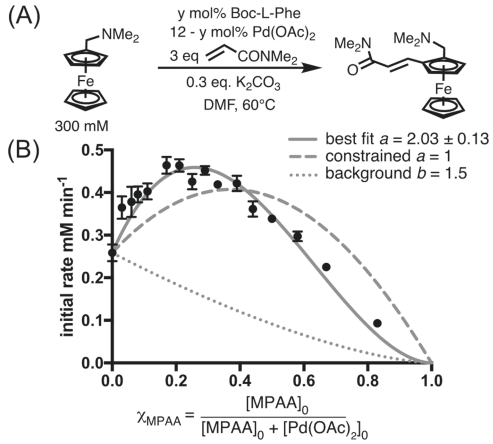

Figure 6. (A) Reaction conditions for kinetic MCV; (B) plot of initial rate of formation of major enantiomer versus χ_{MPAA} with data fit to eq 3, $y = m(\chi_{MPAA})(\chi_{Pd})^a + n(\chi_{Pd})^b$.

The dashed lines in Figure 6 show the poor fit when the model is constrained to 1:1 Pd:MPAA (additional fits and constraints in Figures S71−S73). The best fit for the relative stoichiometry of palladium ($a = 2$) is consistent with our hypothesis, outlined above, that MPAA-accelerated C−H activation can be achieved by a complex with the limiting stoichiometry $Pd_2(MPAA)_1$. As noted above, this does not imply that additional MPAA/carboxylate ligands are not bound to the complex—just that they exert a minimal effect on dmaf olefination rate.

$$\text{initial rate major enantiomer} = m(\chi_{MPAA})(\chi_{Pd})^a + n(\chi_{Pd})^b \quad (3)$$

Computational Evaluation of MPAA-Accelerated Cyclopalladation. Next, DFT calculations were used to study dmaf cyclopalladation in the presence and absence of MPAA ligands.[103] Similar to our previous reports,[36,39,71] here we computed reactants, intermediates, transition states, and products of cyclopalladation via mono-palladium and di-palladium complexes $[Pd_2(X)_2$ and $Pd_2(MPAA)_1(OAc)_1$, where X represents the bridging carboxylates in the reactants and products of the cyclopalladation reaction, X = OAc or MPAA, MPAA = Boc-Gly or Boc-L-Ala]. These calculations indicate that the di-palladium pathways are favored, both kinetically and thermodynamically, relative to the mono-palladium pathways (Figures S151−S154). The computed free energies of species in the second cyclopalladation, relative to their respective pre-reaction complexes (**6**), are shown in Table 1. A representative free energy profile for cyclopalladation of **6** (where MPAA = Boc-L-Ala) is provided in Figure 7. Only the energetically most favorable bridge-ruptured acetate assisted C−H activation pathway is presented here.[36] Similar trends are observed for the first cyclopalladation (Table S20).

The calculated reduction in the barrier for the overall C−H activation process in the presence of Boc-Gly relative to acetate is striking (**6** → **TS**, $\Delta\Delta G^{\ddagger}$ = 7.0 kcal/mol, Table 1). Further analysis reveals that specific stabilization of the activated complex for C−H cleavage only makes up a small fraction of the acceleration (**7** → **TS**, $\Delta\Delta G^{\ddagger}$ = 1.0 kcal/mol, Table 1), whereas most of the stabilization is already present in intermediate **7** (**6** → **7**, $\Delta\Delta G$ = 6.0 kcal/mol, Table 1). Thus, introducing MPAA ligands lowers the barrier to cyclopalladation by stabilizing interactions in the endergonic intermediate (**7**) that are maintained in the C−H activation transition state. Similar results were found for Boc-L-Ala (Table 1).

Table 1. Computed Free Energies (in kcal/mol) of 7 and C−H Cleavage TS Relative to Their Respective Bridged Prereaction Complex 6 for Various Ligands (Acetate, Boc-Gly, and Boc-L-Ala)

		ΔG (kcal/mol)		
complex	X	7	TS	barrier to C−H cleavage[a]
Pd_2X_2	acetate	20.8	29.3	8.5
	Boc-Gly	14.8	22.3	7.5
	Boc-Gly (-HB[b])	19.7	26.8	7.1
	Boc-L-Ala (*S*) (major)	14.9	22.8	7.9
	Boc-L-Ala (*R*) (minor)	18.9	26.5	7.6
$Pd_2X_1OAc_1$	Boc-L-Ala (*S*) (major)	16.2	25.3	9.1
	Boc-L-Ala (*R*) (minor)	17.9	27.2	9.4

[a]kcal/mol. [b]With no hydrogen-bonding (HB) interaction.

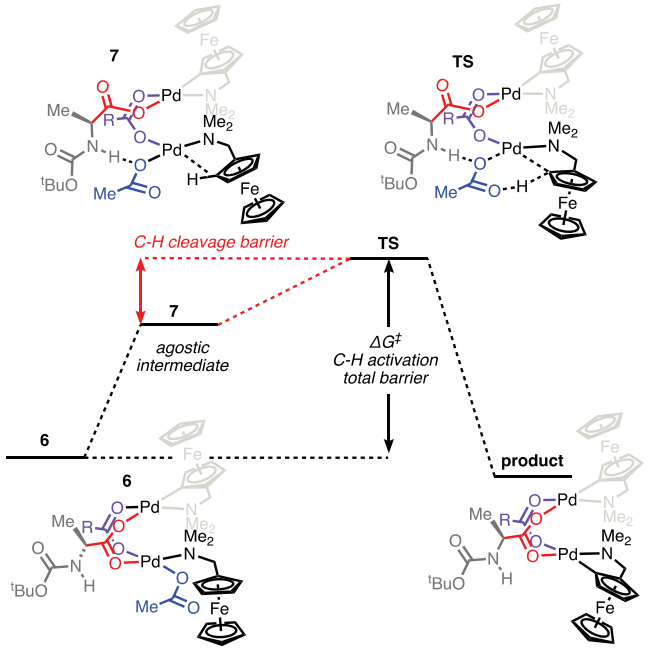

Figure 7. Calculated free energy profile of the second cyclopalladation reaction for the pro-S C−H bond (light gray, substrate from first cyclometallation; black, di-palladium-substrate core; blue, acetate for concerted-metallation-deprotonation; purple, bridging carboxylate; red, bridge-ruptured carboxylate; dark gray, variable side chain on bridge ruptured carboxylate).

A key structural feature of intermediate **7** is hydrogen bonding of the bridge-ruptured MPAA ligand to the acetate participating in concerted metalation deprotonation (CMD). This interaction helps stabilize the reactive bridge-ruptured conformation. To assess the importance of the hydrogen-bonding interaction, structure **7** was re-optimized after manual rotation of the amide group out of close proximity to the CMD transition state so that there would be no hydrogen bonding between the MPAA and the reacting acetate. Removing the hydrogen-bonding interaction between the reactive acetate and

DOI: 10.1021/acscatal.9b03887
ACS Catal. 2019, 9, 11386−11397

NH of Boc-Gly results in an increase in the energy of 7 by 4.9 kcal/mol (labeled Boc-Gly-HB in Table 1, Figure S155). As a result, the overall barrier for Boc-Gly without the hydrogen bonding interaction is higher than that with hydrogen bonding, but still lower than the reaction with acetate. These calculations suggest that hydrogen bonding is a significant (but not sole) factor in acceleration of cyclopalladation by the MPAA ligand.

Building on the ability of the computational model to recapitulate experimentally observed rate acceleration, we next assessed whether the model reproduced observed stereochemical outcomes. The complex with two coordinated MPAA ligands, Pd_2(Boc-L-Ala)$_2$, was examined first because titration studies indicate that this is the most abundant state with standard MPAA loadings used in catalysis (Figures S17–S21). We found lower barriers to activation of both enantiotopic C–H bonds relative to the acetate pathway (consistent with the observed decrease in KIE for both pathways, Figure 4, $\Delta G^{\ddagger}$ acetate = 29.3, $\Delta G^{\ddagger}$ Ala2-R = 26.5, and $\Delta G^{\ddagger}$ Ala2-S = 22.8 kcal/mol). The calculated barriers of the pro-S and pro-R C–H activation are consistent with the *S* chirality of the major product ($\Delta\Delta G^{\ddagger}$ = 3.7 kcal/mol). Most of the $\Delta\Delta G^{\ddagger}$ for pro-S and pro-R selectivity comes from the free energy difference between the pro-S and pro-R agostic complexes 7 ($\Delta\Delta G$ = 4.0 kcal/mol); the difference in the barriers for C–H cleavage is small ($\Delta\Delta G^{\ddagger}$ = 0.3 kcal/mol) (Table 1). Structural analysis of species in the pro-S and pro-R free energy profile show that the key hydrogen-bonding interaction is intact in the pro-S 7 complex (NH–O = 2.07 Å) and disrupted in the disfavored pro-R 7 complex (NH–O = 2.58 Å, Figure S158). These findings indicate that MPAA chirality impacts the hydrogen-bonding interaction, which then effects the extent of acceleration from the MPAA ligand and enantioselectivity. The experimentally observed stereochemical outcomes were borne out in calculations of the first cyclopalladation step as well (Table S20).

Calculations for Pd_2(Boc-L-Ala)$_2$ complexes provide a structural rationale for the observed acceleration of C–H activation and enantioselectivity in the presence of chiral MPAA ligands. The free energy profiles for complexes bearing a single MPAA ligand, Pd_2(Boc-L-Ala)$_1$(OAc)$_1$, were also examined to assess whether the computational model is consistent with the major outcome of this work; namely, that a di-palladium catalyst requires only one MPAA ligand to achieve accelerated C–H functionalization of the major enantiomer relative to minor enantiomer and the acetate-only pathway (Figures S159 and S160). Indeed, replacing one acetate ligand in $Pd_2(AcO)_2$ with Boc-L-Ala lowers the C–H activation barrier of both enantiomers (relative to acetate) and reproduces the absolute chirality of the major reaction product ($\Delta\Delta G^{\ddagger}$ = 1.9 kcal/mol). A hydrogen-bonding interaction is again present in both the intermediate (7) and transition state (Figure 8), and most of the energetic differentiation contributing to enantioselectivity is present in the pro-S and pro-R complexes of 7 ($\Delta\Delta G$ = 1.7 kcal/mol). Overall, the calculations for Pd_2(Boc-L-Ala)$_1$(OAc)$_1$ indicate that a single MPAA ligand can stabilize the high energy intermediate (7) and lower the barrier to enantioselective C–H activation via hydrogen-bonding interactions in the secondary coordination sphere. On the other hand, the calculated barrier to C–H activation at Pd_2(Boc-L-Ala)$_1$(OAc)$_1$ is higher in energy than at Pd_2(Boc-L-Ala)$_2$, suggesting that coordination of a second MPAA ligand should afford faster C–H activation. This

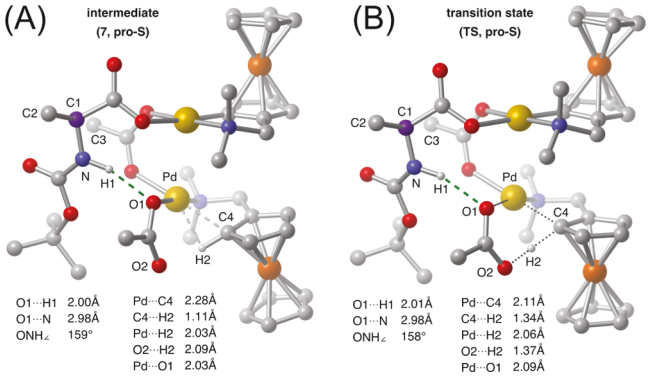

Figure 8. Calculated geometry of (A) intermediate 7 and (B) transition-state **TS** with Boc-L-Ala for the favored enantiomer, pro-S (intramolecular hydrogen-bonding shown with green dashes, Pd = yellow, Fe = orange, O = red, N = blue, C = gray, except MPAA chiral center, C1 = purple, all H's except H1 and H2 were omitted for clarity).

difference in calculated barriers was not expected on the basis of experimental studies, which indicate that only one MPAA ligand is required per di-palladium catalyst for effective acceleration of major enantiomer formation (Figures 5 and 6), but the calculated energy profiles are compatible with at least two specific kinetic scenarios—e.g, faster turnover of MPAA ligands (for accelerating C–H activation) than turnover of the Pd catalyst (for C–H functionalization) or a masked kinetic influence of the second MPAA ligand because of a change in the turnover-limiting step upon coordination of the first MPAA (see further discussion following Figure S160).

As a preliminary test of the computational model of secondary sphere hydrogen bond catalysis, rates and selectivities were compared for reactions conducted with Boc-NH-L-Phe, Boc-NMe-L-Phe, and no MPAA ligands (Figure 9). Under the standard reaction conditions N–Me MPAA accelerates the rate of formation of both major and

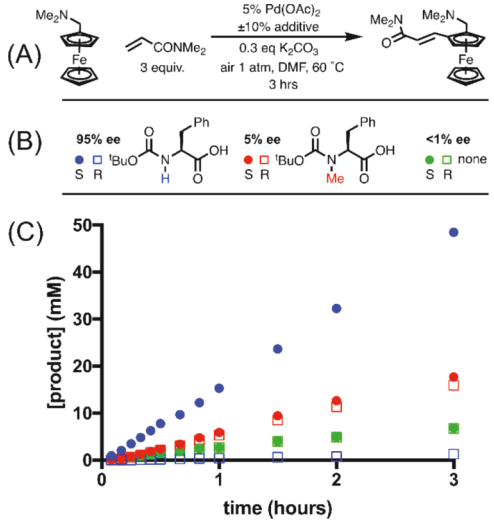

Figure 9. (A) reaction conditions; (B) legend of additives and their corresponding product symbols and enantiomeric excesses; (C) reaction profiles showing total product formation over time in the presence of Boc-NH-Phe (blue), Boc-NMe-Phe (red), and no additive (green) where solid circles indicate major enantiomer and empty squares indicate the minor enantiomer.

DOI: 10.1021/acscatal.9b03887
ACS Catal. 2019, 9, 11386–11397

minor enantiomers, relative to the acetate only reaction, with minimal enantioinduction (5% ee). The hydrogen bonding MPAA ligand afforded even greater rate acceleration and selective acceleration of the major enantiomer (95% ee).

Poor enantioselectivity with N−Me ligands has been observed in other systems and has been interpreted as evidence for the importance of MPAA chelation via nitrogen coordination.[34] The observed acceleration with N−Me MPAA, however, is not compatible with the widely accepted model for Pd−MPAA catalysis via N−H deprotonation and MPAA chelation. The data are consistent with our computational model in which electronic differences between MPAA ligands and acetate contribute to rate acceleration[71,104] while hydrogen bonding interactions afford further rate acceleration and are the dominant factor in controlling enantioselectivity.

MPAA-Accelerated Enantioselective Cyclopalladation of bhp Derivatives. Catalytic reaction kinetics and computational analysis of MPAA promoted cyclopalladation both suggest that a $Pd_2(MPAA)_1$ catalyst lowers the barrier to C−H activation in dmaf olefination. Given the centrality of this step to a range of C−H functionalization reactions,[1] we sought to directly evaluate enantioselective MPAA-accelerated C−H activation without possible complications from other steps in the catalytic cycle by explicitly measuring the effect of MPAA ligands on the rate of cyclopalladation (in the absence of catalyst turnover). Moreover, to evaluate the relevance of $Pd_2(MPAA)_1$ rate acceleration toward other substrates, **8**[34,105,106] was chosen for stoichiometric C−H activation because bhp derivatives are the most frequently studied in computational models of MPAA-promoted cyclopalladation (separated from other steps in catalysis).[22,37−40,107]

Initial rates of cyclopalladation were determined by assaying reaction aliquots quenched with (*S*)-*N*,*N*-dimethylamino-L-phenylalanine (Figure 10A).[18,21,108] The quenching agent halts

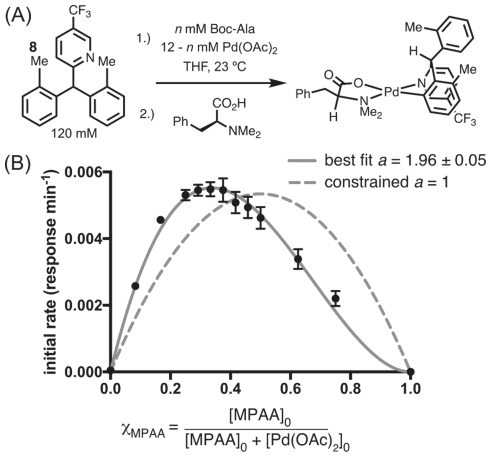

Figure 10. (A) Conditions for kinetic MCV in enantioselective cyclopalladation of **8**; (B) plot of initial rate of major diastereomer formation vs χ_{MPAA} with fits to eq 4.

C−H activation by sequestering unreacted palladium acetate as the bis-chelate (Figure S83). The chelating ligand also simplifies the complex ensemble of cyclopalladation products in solution, leaving two diastereomeric palladacycles (corresponding to enantiomeric products of C−H activation). The relative abundance of each diastereomer was quantified by both ^{19}F NMR spectroscopy and SFC. Both analytical methods indicate the cyclopalladation proceeds in 76−80% ee, which matches the reported ee for palladium-catalyzed C−H functionalization of bhp with Boc-Ala (Figures S80−S86).[34]

$$\text{Initial rate major enantiomer} = m(\chi_{MPAA})(\chi_{Pd})^a \quad (4)$$

The initial rate data obtained from this approach were then analyzed via kinetic MCV to determine the limiting stoichiometry of the transition state of MPAA-accelerated, enantioselective cyclopalladation (Figure 10A). The data in Figure 10B were fit to eq 4, which provided a best fit for the relative stoichiometry of palladium with respect to MPAA of $a = 1.96 \pm 0.05$ (Figure 10B solid curve and Figures S87−S90). A poor fit is obtained when the stoichiometry is constrained to 1:1 Pd:MPAA (Figure 10B, dashed curve). These results indicate that the $Pd_2(MPAA)_1$ species implicated in our structural, kinetic, and computational studies of dmaf olefination are also responsible for MPAA-accelerated C−H activation of bhp. The differences between both the substrates and the conditions used for the dmaf and bhp studies suggest that $Pd_2(MPAA)_1$ complexes could be relevant to a broader range of C−H functionalization reactions involving MPAA ligands than those evaluated in this study.

SUMMARY AND CONCLUSIONS−PROPOSED MECHANISM OF MPAA-ACCELERATED, ENANTIOSELECTIVE DMAF OLEFINATION

The studies outlined above build on structural characterization of MPAA-palladacycles[36] to understand the species responsible for MPAA-accelerated C−H activation of the two substrates that are most frequently employed in models of MPAA-catalysis, dmaf (**1**) and bhp (**8**). Structural, kinetic, and computational analysis provide complementary insights and converge on the significance of complexes with the core structure $Pd_2(MPAA)_1$. The proposed catalytic cycle in Figure 11 summarizes the key observations in this work.

The kinetically competent precatalyst **4** is an acetate-bridged dimer in both the solid state and in solution (Figure 11A). In the presence of excess dmaf, dimer **4** is in equilibrium with the monomer (**9**, Figures S10−S13). A negative order in dmaf suggests that driving the equilibrium toward **9** reduces catalytic activity (Figure 11B). Similar to our previous report,[36] MPAA ligands displace acetate on precatalyst **4**, resulting in an ensemble di-palladium complexes with either one or two coordinated MPAA ligands (Figure 11C).

Moving forward in the productive cycle, the observed first-order rate dependence on olefin concentration (from 0.1 to 1.2 M) demonstrates that olefin insertion contributes to turnover limitation. Saturation kinetics at higher olefin concentrations are consistent with reversible olefin coordination prior to insertion (Figure 11D,E). These data demonstrate the relevance of olefin insertion to the rate of catalyst turnover; however, steps that take place after insertion (β-elimination, O_2 redox chemistry, and ligand exchange) may also contribute to turnover limitation.

Prior competitive KIE experiments have demonstrated that MPAA ligands lower the barrier to C−H activation.[84] The KIEs, measured by absolute rates in separate experiments, presented here, reveal that MPAA ligands can change the turnover limiting step in palladium-catalyzed C−H functionalization.[81] The significant decrease in KIE of dmaf olefination in the presence of MPAA ligands confirms that MPAA-dependent rate acceleration is a result of lower barriers to both enantiotopic C−H bonds cleavage (i.e., those leading to both

DOI: 10.1021/acscatal.9b03887
ACS Catal. 2019, 9, 11386−11397

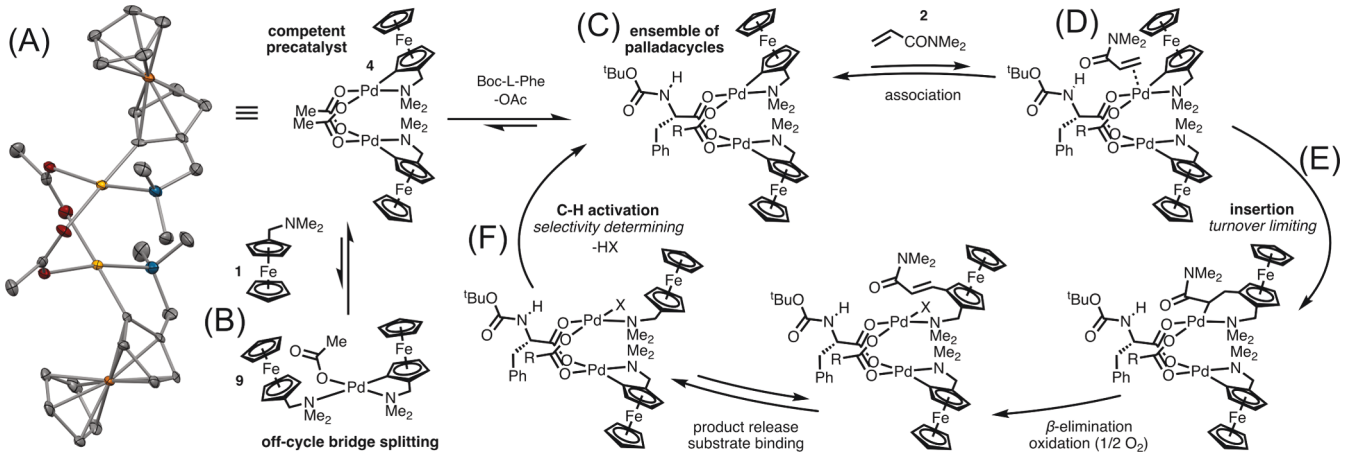

Figure 11. Proposed catalytic cycle for MPAA-accelerated olefination of dmaf.

the major and minor product enantiomers, Figure 11F). The greater decrease in KIE for the reaction leading to formation of the major enantiomer is consistent with selectivity determining C−H activation after turnover-limiting olefin insertion (Figure 4B). On the other hand, this proposal must be reconciled with the observed decrease in the rate of minor product formation with increasing MPAA concentrations (Figure 5). The decrease in both the KIE and the rate of minor enantiomer formation can be explained by a model in which the enantiomeric products are formed through diastereomeric catalysts that are not in rapid equilibrium. In this scenario, the degree of enantioselectivity is determined by the product of the relative concentrations and rate constants of the diastereomeric catalysts.[109−111]

Throughout this work, characterization of palladacycle structure and speciation motivated verifiable hypotheses regarding function. Most notably, observation of $Pd_2(MPAA)_1(OAc)_1$ in equilibrium with $Pd_2(MPAA)_2$ and **4** led us to hypothesize that the essential features of MPAA-catalysis (rate acceleration and enantioselectivity) could be achieved via a transition state containing a bimetallic core bridged by a single MPAA ligand with minimal dependence on a second bridging ligand. In catalytic and stoichiometric reactions (with different substrates, MPAAs, and conditions), kinetic MCV indicates the relevance of $Pd_2(MPAA)_1$ in MPAA-accelerated, enantioselective C−H activation. Moreover, the $Pd_2(MPAA)_1$ model provides a tractable rationale (supported by our computational analysis) for the observed rate acceleration with N−Me ligands (electronic effects) and further acceleration and enantioinduction with N−H ligands (secondary sphere H-bond catalysis). The computational study reproduces experimentally observed rate acceleration, enantioselectivity, and observation of both of these effects with only a single MPAA ligand. It also provides insight into secondary sphere interactions that contribute to rate acceleration and enantioselectivity in these reactions. By identifying active species involved in C−H functionalization reactions catalyzed by Pd−MPAA mixtures, this work provides critical insight into the stabilizing interactions that selectively accelerate desired outcomes and sets the stage for further efforts to design catalysts that harness secondary sphere hydrogen bonding to accelerate di-palladium catalysis.

■ ASSOCIATED CONTENT

Supporting Information

The Supporting Information is available free of charge on the ACS Publications website at DOI: 10.1021/acscatal.9b03887.

Experimental procedures and characterization. These data can be obtained free of charge via www.ccdc.cam.ac.uk/data_request/cif. Computational procedures and supplementary figures (PDF). Tabulated High-Resolution Mass Spectra (CSV). Coordinates of calculated structures (XYZ) (PDF)

CCDC 1865642−1865651 contain the supplementary crystallographic data (CIF)

Details of HRMS bhp (TXT)

Details of HRMS dmaf (TXT)

■ AUTHOR INFORMATION

Corresponding Authors

*E-mail: dmusaev@emory.edu (D.G.M.).

*E-mail: jcl3@iu.edu (J.C.L.).

ORCID

Brandon E. Haines: 0000-0002-5013-8396

Alexander S. Filatov: 0000-0002-8378-1994

Djamaladdin G. Musaev: 0000-0003-1160-6131

Jared C. Lewis: 0000-0003-2800-8330

Notes

The authors declare no competing financial interest.

■ ACKNOWLEDGMENTS

We greatly appreciate the input of CCHF members, including Profs. Jin-Quan Yu, Shannon Stahl, and Donna Blackmond. This work was supported by the NSF under the CCI Center for Selective C-H Functionalization (CCHF, CHE-1700982). JJG was supported by an NSF predoctoral fellowship (DGE-1144082). Use of the Advanced Photon Source, an Office of Science User Facility operated for the U.S. Department of Energy (DOE) Office of Science by Argonne National Laboratory, was supported by U.S. DOE under contract no. DE-AC02-06miltCH11357. ChemMatCARS Sector 15 is principally supported by the Divisions of Chemistry (CHE) and Materials Research (DMR), National Science Foundation, under grant number NSF/CHE-1346572. Use of the Advanced Photon Source, an Office of Science User Facility operated for the U.S. Department of Energy (DOE) Office of Science by

DOI: 10.1021/acscatal.9b03887
ACS Catal. 2019, 9, 11386−11397

Argonne National Laboratory, was supported by the U.S. DOE under contract no. De-AC02-06CH11357. We also gratefully acknowledge the NSF MRI-R2 grant (CHE-0958205 for D.G.M.) and the use of the resources of the Cherry Emerson Center for Scientific Computation.

■ ABBREVIATIONS

MPAA, mono-protected amino acid; bhp, benzhydryl pyridine; dmaf, dimethylaminomethylferrocene; dmba, dimethyl-benzyl-amine; MCV, method of continuous variation; SFC, super-critical fluid chromatography

■ REFERENCES

(1) Berrisford, D. J.; Bolm, C.; Sharpless, K. B. Ligand-Accelerated Catalysis. *Angew. Chem., Int. Ed.* **1995**, *34*, 1059−1070.
(2) Knowles, R. R.; Jacobsen, E. N. Attractive Noncovalent Interactions in Asymmetric Catalysis: Links Between Enzymes and Small Molecule Catalysts. *Proc. Natl. Acad. Sci. U.S.A.* **2010**, *107*, 20678−20685.
(3) Toste, F. D.; Sigman, M. S.; Miller, S. J. Pursuit of Noncovalent Interactions for Strategic Site-Selective Catalysis. *Acc. Chem. Res.* **2017**, *50*, 609−615.
(4) Davis, H. J.; Phipps, R. J. Harnessing Non-Covalent Interactions to Exert Control Over Regioselectivity and Site-Selectivity in Catalytic Reactions. *Chem. Sci.* **2017**, *8*, 864−877.
(5) Engle, K. M. The Mechanism of Palladium(II)-Mediated C−H Cleavage with Mono-N-Protected Amino Acid (MPAA) Ligands: Origins of Rate Acceleration. *Pure Appl. Chem.* **2016**, *88*, 119−138.
(6) Wang, D.-H.; Engle, K. M.; Shi, B.-F.; Yu, J.-Q. Ligand-Enabled Reactivity and Selectivity in a Synthetically Versatile Aryl C-H Olefination. *Science* **2010**, *327*, 315−319.
(7) Leow, D.; Li, G.; Mei, T.-S.; Yu, J.-Q. Activation of Remote Meta-C-H Bonds Assisted by an End-on Template. *Nature* **2012**, *486*, 518−522.
(8) Chan, K. S. L.; Wasa, M.; Chu, L.; Laforteza, B. N.; Miura, M.; Yu, J.-Q. Ligand-Enabled Cross-Coupling of C(Sp3)-H Bonds with Arylboron Reagents via Pd(II)/Pd(0) Catalysis. *Nat. Chem.* **2014**, *6*, 146−150.
(9) Chu, L.; Shang, M.; Tanaka, K.; Chen, Q.; Pissarnitski, N.; Streckfuss, E.; Yu, J.-Q. Remote Meta-C-H Activation Using a Pyridine-Based Template: Achieving Site-Selectivity via the Recognition of Distance and Geometry. *ACS Cent. Sci.* **2015**, *1*, 394−399.
(10) Zhang, Z.; Tanaka, K.; Yu, J.-Q. Remote site-selective C-H activation directed by a catalytic bifunctional template. *Nature* **2017**, *543*, 538−542.
(11) Tang, R.-Y.; Li, G.; Yu, J.-Q. Conformation-Induced Remote Meta-C-H Activation of Amines. *Nature* **2014**, *507*, 215−220.
(12) Zhu, Y.; Chen, X.; Yuan, C.; Li, G.; Zhang, J.; Zhao, Y. Pd-Catalysed Ligand-Enabled Carboxylate-Directed Highly Regioselective Arylation of Aliphatic Acids. *Nat. Commun.* **2017**, *8*, 14904.
(13) Chu, L.; Xiao, K.-J.; Yu, J.-Q. Room-Temperature Enantioselective C-H Iodination via Kinetic Resolution. *Science* **2014**, *346*, 451−455.
(14) Saint-Denis, T. G.; Zhu, R.-Y.; Chen, G.; Wu, Q.-F.; Yu, J.-Q. Enantioselective C(Sp3)−H Bond Activation by Chiral Transition Metal Catalysts. *Science* **2018**, *359*, No. eaao4798.
(15) Zhao, D.; Xu, P.; Ritter, T. Palladium-Catalyzed Late-Stage Direct Arene Cyanation. *Chem* **2019**, *5*, 97−107.
(16) Sokolov, V. I.; Troitskaya, L. L.; Reutov, O. A. Asymmetric Cyclopalladation of Dimethylaminomethylferrocene. *J. Organomet. Chem.* **1979**, *182*, 537−546.
(17) Dendele, N.; Bisaro, F.; Gaumont, A.-C.; Perrio, S.; Richards, C. J. Synthesis of a [2.2]Paracyclophane Based Planar Chiral Palladacycle by a Highly Selective Kinetic Resolution/C−H Activation Reaction. *Chem. Commun.* **2012**, *48*, 1991.
(18) Günay, M. E.; Richards, C. J. Synthesis of Planar Chiral Phosphapalladacycles by N-Acyl Amino Acid Mediated Enantioselective Palladation. *Organometallics* **2009**, *28*, 5833−5836.
(19) Colquhoun, H. M.; Powell, C. T.; Zhu, Z.; Cardin, C. J.; Gan, Y.; Tootell, P.; Tsang, J. S. W.; Boag, N. M. Enantiospecific Assembly of a Homochiral, Hexanuclear Palladium Complex. *Eur. J. Inorg. Chem.* **2009**, *2009*, 999−1002.
(20) Sokolov, V. I.; Troitskaya, L. L.; Khrushchova, N. S. Asymmetric Cyclopalladation in the Ferrocene Series as a Tool for Enantioselective Synthesis. Preparation of Some Analogues of Natural Products. *J. Organomet. Chem.* **1983**, *250*, 439−446.
(21) Komatsu, T.; Nonoyama, M.; Fujita, J. Optical Resolution of Cyclo-Palladated (Dimethylaminomethyl)Ferrocene. *Bull. Chem. Soc. Jpn.* **1981**, *54*, 186−189.
(22) Cheng, G.-J.; Chen, P.; Sun, T.-Y.; Zhang, X.; Yu, J.-Q.; Wu, Y.-D. A Combined IM-MS/DFT Study on [Pd(MPAA)]-Catalyzed Enantioselective C-H Activation: Relay of Chirality Through a Rigid Framework. *Chem.—Eur. J.* **2015**, *21*, 11180−11188.
(23) Gao, D.-W.; Gu, Q.; Zheng, C.; You, S.-L. Synthesis of Planar Chiral Ferrocenes via Transition-Metal-Catalyzed Direct C-H Bond Functionalization. *Acc. Chem. Res.* **2017**, *50*, 351−365.
(24) Gao, D.-W.; Gu, Q.; You, S.-L. An Enantioselective Oxidative C-H/C-H Cross-Coupling Reaction: Highly Efficient Method To Prepare Planar Chiral Ferrocenes. *J. Am. Chem. Soc.* **2016**, *138*, 2544−2547.
(25) Pi, C.; Cui, X.; Liu, X.; Guo, M.; Zhang, H.; Wu, Y. Synthesis of Ferrocene Derivatives with Planar Chirality via Palladium-Catalyzed Enantioselective C-H Bond Activation. *Org. Lett.* **2014**, *16*, 5164−5167.
(26) Gao, D.-W.; Shi, Y.-C.; Gu, Q.; Zhao, Z.-L.; You, S.-L. Enantioselective Synthesis of Planar Chiral Ferrocenes via Palladium-Catalyzed Direct Coupling with Arylboronic Acids. *J. Am. Chem. Soc.* **2013**, *135*, 86−89.
(27) Shi, Y.-C.; Yang, R.-F.; Gao, D.-W.; You, S.-L. Enantioselective Synthesis of Planar Chiral Ferrocenes via Palladium-Catalyzed Annulation with Diarylethynes. *Beilstein J. Org. Chem.* **2013**, *9*, 1891−1896.
(28) Pi, C.; Li, Y.; Cui, X.; Zhang, H.; Han, Y.; Wu, Y. Redox of ferrocene controlled asymmetric dehydrogenative Heck reaction via palladium-catalyzed dual C-H bond activation. *Chem. Sci.* **2013**, *4*, 2675.
(29) Huang, J.; Gu, Q.; You, S. Synthesis of Planar Chiral Ferrocenes via Transition-Metal-Catalyzed Direct C-H Bond Functionalization. *Chin. J. Inorg. Chem.* **2018**, *38*, 51−61.
(30) Schaarschmidt, D.; Lang, H. Selective Syntheses of Planar-Chiral Ferrocenes. *Organometallics* **2013**, *32*, 5668−5704.
(31) Djukic, J.-P.; Hijazi, A.; Flack, H. D.; Bernardinelli, G. Non-Racemic (Scalemic) Planar-Chiral Five-Membered Metallacycles: Routes, Means, and Pitfalls in Their Synthesis and Characterization. *Chem. Soc. Rev.* **2008**, *37*, 406−425.
(32) Günay, M. E.; Ilyashenko, G.; Richards, C. J. Models for the basis of enantioselection in palladium mediated C-H activation reactions. *Tetrahedron: Asymmetry* **2010**, *21*, 2782−2787.
(33) Zhu, D.-Y.; Chen, P.; Xia, J.-B. Synthesis of Planar Chiral Ferrocenes by Transition-Metal-Catalyzed Enantioselective C−H Activation. *ChemCatChem* **2015**, *8*, 68−73.
(34) Shi, B.-F.; Maugel, N.; Zhang, Y.-H.; Yu, J.-Q. PdII-Catalyzed Enantioselective Activation of C(Sp2)-H and C(Sp3)-H Bonds Using Monoprotected Amino Acids as Chiral Ligands. *Angew. Chem., Int. Ed.* **2008**, *47*, 4882−4886.
(35) Navarro, R.; García, J.; Urriolabeitia, E. P.; Cativiela, C.; Diaz-de-Villegas, M. D. Metal Complexes of Biologically Important Ligands: Synthesis of Amino Acidato Complexes of PdII Containing a C,N-Cyclometallated Group as an Ancillary Ligand. *J. Organomet. Chem.* **1995**, *490*, 35−43.
(36) Gair, J. J.; Haines, B. E.; Filatov, A. S.; Musaev, D. G.; Lewis, J. C. Mono- N -Protected Amino Acid Ligands Stabilize Dimeric Palladium(II) Complexes of Importance to C−H Functionalization. *Chem. Sci.* **2017**, *8*, 5746−5756.

DOI: 10.1021/acscatal.9b03887
ACS Catal. 2019, 9, 11386−11397

(37) Musaev, D. G.; Kaledin, A.; Shi, B.-F.; Yu, J.-Q. Key Mechanistic Features of Enantioselective C-H Bond Activation Reactions Catalyzed by [(Chiral Mono-N-Protected Amino Acid)-Pd(II)] Complexes. *J. Am. Chem. Soc.* **2012**, *134*, 1690−1698.
(38) Musaev, D. G.; Figg, T. M.; Kaledin, A. L. Versatile Reactivity of Pd-Catalysts: Mechanistic Features of the Mono-N-Protected Amino Acid Ligand and Cesium-Halide Base in Pd-Catalyzed C−H Bond Functionalization. *Chem. Soc. Rev.* **2014**, *43*, 5009−5031.
(39) Haines, B. E.; Musaev, D. G. Factors Impacting the Mechanism of the Mono-N-Protected Amino Acid Ligand-Assisted and Directing-Group-Mediated C−H Activation Catalyzed by Pd (II) Complex. *ACS Catal.* **2015**, *5*, 830−840.
(40) Haines, B. E.; Yu, J.-Q.; Musaev, D. G. Enantioselectivity Model for Pd-Catalyzed C−H Functionalization Mediated by the Mono-N-Protected Amino Acid (MPAA) Family of Ligands. *ACS Catal.* **2017**, *7*, 4344−4354.
(41) Cheng, G.-J.; Yang, Y.-F.; Liu, P.; Chen, P.; Sun, T.-Y.; Li, G.; Zhang, X.; Houk, K. N.; Yu, J.-Q.; Wu, Y.-D. Role of N-Acyl Amino Acid Ligands in Pd(II)-Catalyzed Remote C-H Activation of Tethered Arenes. *J. Am. Chem. Soc.* **2014**, *136*, 894−897.
(42) Cheng, G.-J.; Chen, P.; Sun, T.-Y.; Zhang, X.; Yu, J.-Q.; Wu, Y.-D. A Combined IM-MS/DFT Study on [Pd(MPAA)]-Catalyzed Enantioselective C-H Activation: Relay of Chirality Through a Rigid Framework. *Chem.—Eur. J.* **2015**, *21*, 11180−11188.
(43) Zhong, X.-M.; Cheng, G.-J.; Chen, P.; Zhang, X.; Wu, Y.-D. Mechanistic Study on Pd/Mono-N-Protected Amino Acid Catalyzed Vinyl-Vinyl Coupling Reactions: Reactivity and E/Z Selectivity. *Org. Lett.* **2016**, *18*, 5240−5243.
(44) Fang, S.; Wang, X.; Yin, F.; Cai, P.; Yang, H.; Kong, L. Palladium-Catalyzed Meta-C-H Olefination of Arene-Tethered Diols Directed by Well-Designed Pyrimidine-Based Group. *Org. Lett.* **2019**, *21*, 1841−1844.
(45) Jayarajan, R.; Das, J.; Bag, S.; Chowdhury, R.; Maiti, D. Diverse meta -C−H Functionalization of Arenes across Different Linker Lengths. *Angew. Chem., Int. Ed.* **2018**, *57*, 7659−7663.
(46) Baxter, R. D.; Sale, D.; Engle, K. M.; Yu, J.-Q.; Blackmond, D. G. Mechanistic Rationalization of Unusual Kinetics in Pd-Catalyzed C-H Olefination. *J. Am. Chem. Soc.* **2012**, *134*, 4600−4606.
(47) Plata, R. E.; Hill, D. E.; Haines, B. E.; Musaev, D. G.; Chu, L.; Hickey, D. P.; Sigman, M. S.; Yu, J.-Q.; Blackmond, D. G. A Role for Pd(IV) in Catalytic Enantioselective C-H Functionalization with Monoprotected Amino Acid Ligands Under Mild Conditions. *J. Am. Chem. Soc.* **2017**, *139*, 9238−9245.
(48) Hill, D. E.; Bay, K. L.; Yang, Y.-F.; Plata, R. E.; Takise, R.; Houk, K. N.; Yu, J.-Q.; Blackmond, D. G. Dynamic Ligand Exchange as a Mechanistic Probe in Pd-Catalyzed Enantioselective C−H Functionalization Reactions Using Monoprotected Amino Acid Ligands. *J. Am. Chem. Soc.* **2017**, *139*, 18500−18503.
(49) Hill, D. E.; Pei, Q.-L.; Zhang, E.-X.; Gage, J. R.; Yu, J.-Q.; Blackmond, D. G. A General Protocol for Addressing Speciation of the Active Catalyst Applied to Ligand-Accelerated Enantioselective C(Sp 3)−H Bond Arylation. *ACS Catal.* **2018**, *8*, 1528−1531.
(50) Chen, X.; Engle, K. M.; Wang, D.-H.; Yu, J.-Q. Palladium(II)-Catalyzed C-H Activation/C-C Cross-Coupling Reactions: Versatility and Practicality. *Angew. Chem., Int. Ed.* **2009**, *48*, 5094−5115.
(51) Wencel-Delord, J.; Colobert, F. Asymmetric C(Sp2)-H Activation. *Chem.—Eur. J.* **2013**, *19*, 14010−14017.
(52) Engle, K. M.; Yu, J.-Q. Developing Ligands for Palladium(II)-Catalyzed C-H Functionalization: Intimate Dialogue Between Ligand and Substrate. *J. Org. Chem.* **2013**, *78*, 8927−8955.
(53) Zheng, C.; You, S.-L. Recent Development of Direct Asymmetric Functionalization of Inert C−H Bonds. *RSC Adv.* **2014**, *4*, 6173.
(54) Zhang, X.; Chung, L. W.; Wu, Y.-D. New Mechanistic Insights on the Selectivity of Transition-Metal-Catalyzed Organic Reactions: the Role of Computational Chemistry. *Acc. Chem. Res.* **2016**, *49*, 1302−1310.
(55) Newton, C. G.; Wang, S.-G.; Oliveira, C. C.; Cramer, N. Catalytic Enantioselective Transformations Involving C-H Bond Cleavage by Transition-Metal Complexes. *Chem. Rev.* **2017**, *117*, 8908−8976.
(56) Davies, D. L.; Macgregor, S. A.; McMullin, C. L. Computational Studies of Carboxylate-Assisted C-H Activation and Functionalization at Group 8-10 Transition Metal Centers. *Chem. Rev.* **2017**, *117*, 8649−8709.
(57) Yang, Y.-F.; Hong, X.; Yu, J.-Q.; Houk, K. N. Experimental-Computational Synergy for Selective Pd(II)-Catalyzed C-H Activation of Aryl and Alkyl Groups. *Acc. Chem. Res.* **2017**, *50*, 2853−2860.
(58) Liao, G.; Zhou, T.; Yao, Q.-J.; Shi, B.-F. Recent Advances in the Synthesis of Axially Chiral Biaryls via Transition Metal-Catalysed Asymmetric C-H Functionalization. *Chem. Commun.* **2019**, *55*, 8514−8523.
(59) Dey, A.; Sinha, S. K.; Achar, T. K.; Maiti, D. Accessing Remote Meta- and Para-C(Sp2)-H Bonds with Covalently Attached Directing Groups. *Angew. Chem., Int. Ed. Engl.* **2019**, *58*, 10820−10843.
(60) Cheng, G.-J.; Zhong, X.-M.; Wu, Y.-D.; Zhang, X. Mechanistic Understanding of Catalysis by Combining Mass Spectrometry and Computation. *Chem. Commun.* **2019**, *55*, 12749−12764.
(61) Váňa, J.; Hanusek, J.; Sedlák, M. Bi and Trinuclear Complexes in Palladium Carboxylate-Assisted C-H Activation Reactions. *Dalton Trans.* **2018**, *47*, 1378−1382.
(62) Pakula, R. J.; Srebro-Hooper, M.; Fry, C. G.; Reich, H. J.; Autschbach, J.; Berry, J. F. Palladium Acetate Revisited: Unusual Ring-Current Effects, One-Electron Reduction, and Metal-Metal Bonding. *Inorg. Chem.* **2018**, *57*, 8046−8049.
(63) Váňa, J.; Lang, J.; Šoltésová, M.; Hanusek, J.; Růžička, A.; Sedlák, M.; Roithová, J. The Role of Trinuclear Species in a Palladium Acetate/Trifluoroacetic Acid Catalytic System. *Dalton Trans.* **2017**, *46*, 16269−16275.
(64) Hruszkewycz, D. P.; Wu, J.; Hazari, N.; Incarvito, C. D. Palladium(I)-Bridging Allyl Dimers for the Catalytic Functionalization of CO2. *J. Am. Chem. Soc.* **2011**, *133*, 3280−3283.
(65) Efimenko, I. A.; Podobedov, R. E.; Churakov, A. V.; Kuz'mina, L. G.; Garbuzova, I. A.; Lokshin, B. V.; Maksimov, A. L.; Flid, V. R. Binary Palladium Carboxylates with Electron-Donating and Electron-Withdrawing Substituents in the Carboxylate Ligand: Synthesis and Structural Studies. the Crystal Structures of Pd3(M-CH2ClCO2)6 · CH2Cl2, Pd3(M-C6H11CO2)6, and Pd3(M-CMe3CO2)6. *Russ. J. Coord. Chem.* **2011**, *37*, 625−634.
(66) Stromnova, T. A.; Monakhov, K. Y.; Cámpora, J.; Palma, P.; Carmona, E.; Alvarez, E. Synthesis and Solution Behavior of the Trinuclear Palladium(II) Unsaturated Carboxylate Complexes Triangle-Pd3[M-O2CC(R′)=CHMe]6 (R′=Me, H): X-Ray Structure of Palladium(II) Tiglate (R′=Me). *Inorg. Chim. Acta* **2007**, *360*, 4111−4116.
(67) Skapski, A. C.; Smart, M. L. The Crystal Structure of Trimeric Palladium(II) Acetate. *J. Chem. Soc. D* **1970**, 658b.
(68) Powers, D. C.; Ritter, T. Bimetallic Redox Synergy in Oxidative Palladium Catalysis. *Acc. Chem. Res.* **2012**, *45*, 840−850.
(69) Kornecki, K. P.; Berry, J. F.; Powers, D. C.; Ritter, T. Metal-Metal Bond-Containing Complexes as Catalysts for C-H Functionalization. *Progress in Inorganic Chemistry*; John Wiley & Sons, Inc.: Hoboken, New Jersey, 2014; Vol. *58*, pp 225−302.
(70) Bedford, R. B.; Bowen, J. G.; Davidson, R. B.; Haddow, M. F.; Seymour-Julen, A. E.; Sparkes, H. A.; Webster, R. L. Facile Hydrolysis and Alcoholysis of Palladium Acetate. *Angew. Chem., Int. Ed.* **2015**, *54*, 6591−6594.
(71) Haines, B. E.; Berry, J. F.; Yu, J.-Q.; Musaev, D. G. Factors Controlling Stability and Reactivity of Dimeric Pd(II) Complexes in C-H Functionalization Catalysis. *ACS Catal.* **2016**, *6*, 829−839.
(72) Haines, B. E.; Xu, H.; Verma, P.; Wang, X.-C.; Yu, J.-Q.; Musaev, D. G. Mechanistic Details of Pd(II)-Catalyzed C-H Iodination with Molecular I2: Oxidative Addition vs Electrophilic Cleavage. *J. Am. Chem. Soc.* **2015**, *137*, 9022−9031.
(73) Wang, D.; Weinstein, A. B.; White, P. B.; Stahl, S. S. Ligand-Promoted Palladium-Catalyzed Aerobic Oxidation Reactions. *Chem. Rev.* **2018**, *118*, 2636−2679.

DOI: 10.1021/acscatal.9b03887
ACS Catal. 2019, 9, 11386−11397

(74) Blackmond, D. G. Reaction Progress Kinetic Analysis: a Powerful Methodology for Mechanistic Studies of Complex Catalytic Reactions. *Angew. Chem., Int. Ed.* **2005**, *44*, 4302−4320.
(75) Ryabov, A. D. Thermodynamics, Kinetics, and Mechanism of Exchange of Cyclopalladated Ligands Ic00255a015. *Inorg. Chem.* **1987**, *26*, 1252−1260.
(76) Milani, J.; Pridmore, N. E.; Whitwood, A. C.; Fairlamb, I. J. S.; Perutz, R. N. The Role of Fluorine Substituents in the Regioselectivity of Intramolecular C-H Bond Functionalization of Benzylamines at Palladium(II). *Organometallics* **2015**, *34*, 4376−4386.
(77) Deprez, N. R.; Sanford, M. S. Synthetic and Mechanistic Studies of Pd-Catalyzed C−H Arylation with Diaryliodonium Salts: Evidence for a Bimetallic High Oxidation State Pd Intermediate. *J. Am. Chem. Soc.* **2009**, *131*, 11234−11241.
(78) Powers, D. C.; Xiao, D. Y.; Geibel, M. A. L.; Ritter, T. On the Mechanism of Palladium-Catalyzed Aromatic C−H Oxidation. *J. Am. Chem. Soc.* **2010**, *132*, 14530−14536.
(79) Campbell, C. T. The Degree of Rate Control: a Powerful Tool for Catalysis Research. *ACS Catal.* **2017**, *7*, 2770−2779.
(80) Johnson, K. A.; Goody, R. S. The original Michaelis constant: translation of the 1913 Michaelis-Menten paper. *Biochemistry* **2011**, *50*, 8264−8269.
(81) Simmons, E. M.; Hartwig, J. F. On the Interpretation of Deuterium Kinetic Isotope Effects in C-H Bond Functionalizations by Transition-Metal Complexes. *Angew. Chem., Int. Ed.* **2012**, *51*, 3066−3072.
(82) Algera, R. F.; Gupta, L.; Hoepker, A. C.; Liang, J.; Ma, Y.; Singh, K. J.; Collum, D. B. Lithium Diisopropylamide: Non-equilibrium Kinetics and Lessons Learned About Rate Limitation. *J. Org. Chem.* **2017**, *82*, 4513−4532.
(83) Engle, K. M.; Wang, D.-H.; Yu, J.-Q. Ligand-Accelerated C−H Activation Reactions: Evidence for a Switch of Mechanism. *J. Am. Chem. Soc.* **2010**, *132*, 14137−14151.
(84) Engle, K. M.; Wang, D.-H.; Yu, J.-Q. Ligand-Accelerated C−H Activation Reactions: Evidence for a Switch of Mechanism. *J. Am. Chem. Soc.* **2010**, *132*, 14137−14151.
(85) Thuy-Boun, P. S.; Villa, G.; Dang, D.; Richardson, P.; Su, S.; Yu, J.-Q. Ligand-Accelerated ortho-C-H Alkylation of Arylcarboxylic Acids using Alkyl Boron Reagents. *J. Am. Chem. Soc.* **2013**, *135*, 17508−17513.
(86) Noble-Terán, M. E.; Buhse, T.; Cruz, J.-M.; Coudret, C.; Micheau, J.-C. Nonlinear Effects in Asymmetric Synthesis: a Practical Tool for the Discrimination Between Monomer and Dimer Catalysis. *ChemCatChem* **2016**, *8*, 1836−1845.
(87) Satyanarayana, T.; Abraham, S.; Kagan, H. B. Nonlinear Effects in Asymmetric Catalysis. *Angew. Chem., Int. Ed.* **2009**, *48*, 456−494.
(88) Kennedy, C. R. Mechanistic Studies in Enantioselective Ion-Pairing Catalysis with Dual Hydrogen-Bond Donors. Ph.D. Thesis, Harvard University, Cambridge, MA, 2016, pp 30−34.
(89) Renny, J. S.; Tomasevich, L. L.; Tallmadge, E. H.; Collum, D. B. Method of Continuous Variations: Applications of Job Plots to the Study of Molecular Associations in Organometallic Chemistry. *Angew. Chem., Int. Ed.* **2013**, *52*, 11998−12013.
(90) Ma, Y.; Hoepker, A. C.; Gupta, L.; Faggin, M. F.; Collum, D. B. 1,4-Addition of Lithium Diisopropylamide to Unsaturated Esters: Role of Rate-Limiting Deaggregation, Autocatalysis, Lithium Chloride Catalysis, and Other Mixed Aggregation Effects. *J. Am. Chem. Soc.* **2010**, *132*, 15610−15623.
(91) Gupta, L.; Hoepker, A. C.; Ma, Y.; Viciu, M. S.; Faggin, M. F.; Collum, D. B. Lithium Diisopropylamide-Mediated Ortholithiation of 2-Fluoropyridines: Rates, Mechanisms, and the Role of Autocatalysis. *J. Org. Chem.* **2013**, *78*, 4214−4230.
(92) Shevlin, M.; Friedfeld, M. R.; Sheng, H.; Pierson, N. A.; Hoyt, J. M.; Campeau, L.-C.; Chirik, P. J. Nickel-Catalyzed Asymmetric Alkene Hydrogenation of A,B-Unsaturated Esters: High-Throughput Experimentation-Enabled Reaction Discovery, Optimization, and Mechanistic Elucidation. *J. Am. Chem. Soc.* **2016**, *138*, 3562−3569.
(93) Nielsen, L. P. C.; Stevenson, C. P.; Blackmond, D. G.; Jacobsen, E. N. Mechanistic Investigation Leads to a Synthetic Improvement in the Hydrolytic Kinetic Resolution of Terminal Epoxides. *J. Am. Chem. Soc.* **2004**, *126*, 1360−1362.
(94) Huang, C. Y. [27] Determination of binding stoichiometry by the continuous variation method: The job plot. *Methods Enzymol.* **1982**, *87*, 509−525.
(95) Doiuchi, T.; Yamaguchi, H.; Minoura, Y. Cyclocopolymerization of D-Limonene with Maleic Anhydride. *Eur. Polym. J.* **1981**, *17*, 961−968.
(96) Sigman, D. S.; Jorgensen, C. T. Models for Metalloenzymes. Zinc (II)-Catalyzed Transesterification of N-(B-Hydroxyethyl)-Ethylenediamine by P-Nitrophenyl Picolinate. *J. Am. Chem. Soc.* **1972**, *94*, 1724−1730.
(97) Prince, R. H.; Woolley, P. R. Metal-ion assisted catalysis of nucleophilic attack. Part I. Zinc-anion co-operation in aldehyde hydration. *J. Chem. Soc., Dalton Trans.* **1972**, 1548−1554.
(98) Wang, L.; Ye, Y.; Lykourinou, V.; Angerhofer, A.; Ming, L.-J.; Zhao, Y. Metal Complexes of a Multidentate Cyclophosphazene with Imidazole-Containing Side Chains for Hydrolyses of Phosphoesters - Bimolecular vs. Intramolecular Dinuclear Pathway. *Eur. J. Inorg. Chem.* **2011**, *2011*, 674−682.
(99) Wang, L.; Ye, Y.; Lykourinou, V.; Yang, J.; Angerhofer, A.; Zhao, Y.; Ming, L.-J. Catalytic Cooperativity, Nuclearity, and O 2/H 2O 2Specificity of Multi-Copper(II) Complexes of Cyclen-Tethered Cyclotriphosphazene Ligands in Aqueous Media. *Eur. J. Inorg. Chem.* **2017**, *2017*, 4899−4908.
(100) Lönnberg, T. A.; Helkearo, M.; Jancsó, A.; Gajda, T. Mimics of Small Ribozymes Utilizing a Supramolecular Scaffold. *Dalton Trans.* **2012**, *41*, 3328.
(101) Song, Y.; Han, X.; Guo, X.; Zeng, Q.; Jiang, F. Metallovesicular Catalytic Hydrolysis of P-Nitrophenyl Picolinate Catalyzed by Zinc(II) Complexes of Pyridyl Ligands in Vesicular Solution. *Colloids Surf., A* **2011**, *392*, 110−115.
(102) Tay, W. M.; Epperson, J. D.; da Silva, G. F. Z.; Ming, L.-J. 1H NMR, Mechanism, and Mononuclear Oxidative Activity of the Antibiotic Metallopeptide Bacitracin: the Role of D-Glu-4, Interaction with Pyrophosphate Moiety, DNA Binding and Cleavage, and Bioactivity. *J. Am. Chem. Soc.* **2010**, *132*, 5652−5661.
(103) Energies Are Reported at the B3LYP-D3BJ/6-311+G(2d,P) and SDD for Pd, Fe (W/ECP)//B3LYP-D3BJ/6-31G(D,P) and LANL2DZ for Pd, Fe (W/ECP) Level of Theory with Bulk Solvent Effects Incorporated with the PCM Implicit Solvation Model for DMF. All Calculations Were Performed with the Gaussian 09 Electronic Structure Package. See Supporting Information for Full Computational Details and References.
(104) Váňa, J.; Bartacek, J.; Hanusek, J.; Roithová, J.; Sedlák, M. C-H Functionalizations by Palladium Carboxylates: the Acid Effect. *J. Org. Chem.* **2019**, *84*, 12746−12754.
(105) Canty, A. J.; Minchin, N. J.; Skelton, B. W.; White, A. H. Interaction of Palladium(II) Acetate with Substituted Pyridines, Including a Cyclometallation Reaction and the Structure of $[Pd\{Meso\text{-}[(Py)PhMeC]_2\text{-}C_5H_3N\}(O_2CMe)][O_2CMe]\cdot 3H_2O$. *J. Chem. Soc., Dalton Trans.* **1986**, 2205−2210.
(106) Fuchita, Y. Fuchita JACS 1981 Preparation and Characterization of Novel Six Membered Cyclopalladated Complexes of 2-Benzylpyridine Ic50226a057. *Inorg. Chem.* **1982**, *20*, 4316−4320.
(107) Park, Y.; Niemeyer, Z. L.; Yu, J.-Q.; Sigman, M. S. Quantifying Structural Effects of Amino Acid Ligands in Pd(II)-Catalyzed Enantioselective C-H Functionalization Reactions. *Organometallics* **2018**, *37*, 203−210.
(108) Dunina, V. V.; Razmyslova, E. D.; Kuz'mina, L. G.; Churakov, A. V.; Rubina, M. Y.; Grishin, Y. K. Synthesis and resolution of an α-phenyl substituted ortho-palladated matrix. *Tetrahedron: Asymmetry* **1999**, *10*, 3147−3155.
(109) Blackmond, D. G.; Rosner, T.; Neugebauer, T.; Reetz, M. T. Kinetic Influences on Enantioselectivity for Non-Diastereopure Catalyst Mixtures. *Angew. Chem., Int. Ed.* **1999**, *38*, 2196−2199.
(110) Beak, P.; Anderson, D. R.; Curtis, M. D.; Laumer, J. M.; Pippel, D. J.; Weisenburger, G. A. Dynamic Thermodynamic

DOI: 10.1021/acscatal.9b03887
ACS Catal. 2019, 9, 11386−11397

Resolution: Control of Enantioselectivity Through Diastereomeric Equilibration. *Acc. Chem. Res.* **2000**, *33*, 715−727.
(111) Buono, F.; Walsh, P. J.; Blackmond, D. G. Rationalization of Anomalous Nonlinear Effects in the Alkylation of Substituted Benzaldehydes. *J. Am. Chem. Soc.* **2002**, *124*, 13652−13653.

DOI: 10.1021/acscatal.9b03887
ACS Catal. 2019, 9, 11386−11397